On the use of ground-motion simulations within ShakeMap methodology: application to the 2008 Iwate-Miyagi Nairiku (Japan) and 1980 Irpinia (Italy) earthquakes

Cultrera G.[1], G. Ameri[1], A. Saraò[2], A. Cirella[1], A. Emolo[3]

[1] *Istituto Nazionale di Geofisica e Vulcanologia, Italy*

[2] *Istituto Nazionale di Oceanografia e Geofisica Sperimentale, Trieste, Italy*

[3] *Dipartimento di Scienze Fisiche, Università Federico II, Napoli, Italy*

Abstract

ShakeMap package uses empirical Ground Motion Prediction Equations (GMPEs) to estimate the ground motion where recorded data are not available. Recorded and estimated values are then interpolated in order to produce a shaking map associated with the seismic event of interest. The ShakeMap approach better works in regions with dense stations coverage, where the observed ground motions adequately constrain the interpolation. In poorly instrumented regions, the ground motion estimate mainly relies on the GMPE, that account only for average characteristics of source and wave propagation processes.

In this study we investigated the improvement of ShakeMap in the near fault area when including synthetic estimates. We focus on the 2008, Mw 7.0, Iwate-Miyagi Nairiku (Japan) earthquake as a case study because recorded by a huge number of stations. As first we calculated the shakemaps to be used as reference maps and then removed several subsets of stations from the original data-set, replacing them with: (*i*) the estimations of the ground motion obtained by using a specific GMPE valid for that area, using simple source information such as the earthquake magnitude and fault geometry; (*ii*) the peak values from synthetic time-histories computed with a hybrid deterministic-stochastic method for extended fault, using the rupture fault model obtained from the kinematic source inversion of strong-motion records.

We evaluate the deviations from the reference map and the sensitivity to the number of sites where recordings are not available. Our results show that shakemaps are more and more reliable as the coverage of stations is dense and uniformly distributed in the near-source area. Moreover, the synthetics account for propagation and source properties in a more correct way than GMPE, and largely improve the results. The hybrid maps reach good fitting levels especially when synthetics are used to integrate real data and for particular strong-motion parameters and stations' distribution.

1. Introduction

Rapid characterization of near-fault strong ground-shaking is essential for assessment of earthquake's impact, including damages and losses estimation. ShakeMap (Wald et al., 1999) was developed as a tool to provide contour maps of the various ground motion parameters, and it has proven to be a valuable information resource for seismologists, emergency response agencies and general public. Immediately after an earthquake the ShakeMap software is routinely run at USGS using data from local U.S. and/or global networks and maps are organized in a data-base available on the World Wide Web. Recently, the Italian Civil Protection Department has supported the ShakeMap implementation in Italy, and the ShakeMap software is at present fully operative at the Istituto Nazionale di Geofisica e Vulcanologia (Michelini et al., 2008) as well as at other Italian seismological institutions (Moratto et al., 2009; Iannaccone et al., 2010; Bragato et al., 2011; Emolo et al., 2011).

To generate a shakemap, observed ground motion parameters (generally PGV, PGA, PSA at different periods) are interpolated with estimates obtained through empirical Ground Motion Prediction Equations (GMPEs) at sites where instrumental data are not available. The ShakeMap approach better works in regions with dense stations coverage, where the observed ground motions adequately constrain the interpolation. In poorly instrumented regions or in cases where the data are lost (for instance, due to signal saturation), the shakemaps mainly rely on the GMPE estimates. At a first approximation, the GMPEs are based on the earthquake magnitude and epicentral or hypocentral distance. However, in case of large earthquakes, the strongest shaking area is very likely not co-located with the epicenter due to the actual extent of the fault rupture and GMPEs based on the distance to the fault rupture are more appropriate. Once these additional information are available, it is possible to account for fault dimension/position and the dominant rupture direction and, within few hours, for the rupture process on the fault plane as computed with the inversion of the recorded seismograms. The increasing information on the seismic source allows the implementation of ShakeMap to account for the effects of fault finiteness on the expected ground motion at different levels (Convertito et al., 2011; Faenza et al., 2011; Spagnuolo, 2010 and Spagnuolo et al., 2010). In particular, Convertito et al. (2011) propose a methodology to infer the surface fault projection and the dominant rupture direction from the inversion of observed PGA and PGV. Faenza et al. (2011) verify that only after the insertion of the finite fault within the shakemaps calculation, the maps appear to replicate more faithfully the level of ground motion indicated by the reported macroseismic field of the 2009, L'Aquila earthquake. Finally, Spagnuolo (2010) and Spagnuolo et al. (2010) investigate the possibility to include in the ShakeMap the GMPE correction factor for the directivity effect (Spudich and Chiou, 2008), able to account for the source complexity.

Several authors (e.g., Dreger et al., 2005; Moratto et al., 2009; Rhie et al., 2009; Moratto and Saraò, 2011, among many others) already tried to use synthetic ground motions and/or to integrate recorded data, empirical GMPE and synthetic values to improve ShakeMap in the vicinity of the seismic source. The possibility of improving the ShakeMap performance by including source

effects and synthetics is particularly appealing in active seismic areas where, in general, the strong-motion station coverage might not be good enough to ensure a correct evaluation of the shaking close to the fault for moderate-to-large earthquakes. For instance in Italy, the first shakemaps for the 2009 L'Aquila (Mw6.3, central Italy) earthquake generated timely after the mainshock could not account for data close to the epicenter for some technical reason (saturation of broad band within 80 km and delay in data transmission of the RAN accelerometric network, see Faenza et al., 2011, for details). For that earthquake Moratto and Saraò (2011) demonstrated that the integration of real data with synthetics could have decreased discrepancies between computed and actual ground shaking maps, mainly in the near field zone where the observed damage was relevant.

In this study we aim at systematically assessing the improvement of ShakeMap when accounting for source effects, at different level of approximation, and including synthetic estimates at sites where recordings are not available. To achieve our goal we need to play an academic exercise on a well instrumented earthquake with a good station coverage. As case study we chose the Mw 7.0, 2008 Iwate-Miyagi Nairiku (Japan) earthquake whose shakemaps were well constrained by real data. In this way we had reliable reference shakemaps to compare with the shakemaps that we generated integrating real data and GMPE with synthetics (hybrid shakemaps).

At the beginning of our investigation, the simple information of the fault geometry were used to evaluate the ground motion at the recording sites using a GMPE derived for the area (Kanno et al., 2006). Then, we used the rupture model retrieved by kinematic source inversion of strong-motion records to simulate the shaking motion through a hybrid deterministic-stochastic approach. An advantage of using simulated motions from kinematic rupture models is that source effects, as rupture directivity, are directly included in the synthetics.

Finally, we show an application of the hybrid shakemaps to the Ms 6.9 1980 Irpinia (Southern Italy) earthquake, in order to validate the improvement in the ground motion estimates for a poorly instrumented earthquake.

2. Data and methodology

The 2008, Mw 7.0, Iwate-Miyagi Nairiku earthquake was recorded by the dense strong motion seismic networks KiK-net (http://www.kik.bosai.go.jp) and K-NET (http://www.k-net.bosai.go.jp), operated by the National Research Institute for Earth Science and Disaster Prevention (NIED). In this study we used accelerometric records from stations located at epicentral distances ranging from 6.3 km to180 km, selecting 66 K-NET and 50 Kik-net stations (Figure 1).

First of all, using a selected set of stations (circles in the figure 1), we retrieved the rupture fault model for the earthquake. Then, we calculated the shakemaps to be used as reference maps using the whole available data-set. Subsequently, we removed several subsets of stations from the original data-set following specific criteria as described in details hereinafter, replacing them with: (*i*) estimations of the ground motion obtained by using the specific GMPE valid for that area (Kanno et

al., 2006), knowing some basic information such as the earthquake magnitude and fault geometry (Test 1); (*ii*) ground motion parameters extracted from synthetic time-histories computed using a hybrid deterministic-stochastic method for extended fault (Test 2). This technique requires a rupture source model, that, as said before, we retrieved from the inversion of selected strong-motion waveforms.

2.1 Strong motion data and rupture history of the 2008 Iwate-Miyagi Nairiku earthquake

The Mw 7.0 Iwate-Miyagi Nairiku earthquake occurred on 2008, June 13 (23:43:49.7 UTC) in the Honshu Island in Japan, activating a reverse fault (Figure 1). The distinction of the rupture plane from the auxiliary one has been debated in the literature. However, Suzuki et al. (2010) pointed out that the distribution of the surface rupture had a NNE-SSW trend similar to the aftershocks distribution, indicating a west-dipping fault plane.

We imaged the rupture history of the 2008 Iwate-Miyagi Nairiku earthquake using seismograms from 11 borehole stations of KiK-net and 2 surface stations of K-NET with epicentral distances less than 70 km (Figure 1). The small number of stations has been chosen in the hypothesis of few recordings available in the near-source region. The adopted non-linear kinematic inversion technique (Piatanesi et al., 2007; Cirella et al., 2008) allowed us to retrieve a complete kinematic description of the source process on the fault plane. Original acceleration recordings have been integrated to obtain ground velocity time-histories and then band-pass filtered between 0.0 and 0.5 Hz using a two-poles two-passes Butterworth filter. We inverted 60 seconds of each waveform, including body and surface waves assuming a planar fault model with a 40° dip and that extends about 44.4km in the strike direction (N209°E) and about 19km in the dip direction (Figure 1). The rupture starting point is located at (39.027° N, 140.878° E) at a depth of 6.5 km, according to the hypocenter proposed by Suzuki et al. (2010).

All the source kinematic parameters were simultaneously inverted at a set of nodal points equally spaced (each 3.17 km) both along strike and dip directions. The searching algorithm explored about 2 millions of rupture models to build-up the model ensemble: the peak slip-velocity was allowed to vary between 0 and 7.5 m/s with 0.25 m/s step increment; the possible rise-time values were selected between 1 and 4 s with 0.25s step increment; the rake angle ranged between 84° and 124° with 5° step increment; finally, the rupture time distribution was constrained by a rupture velocity ranging between 1.6 and 2.4 km/s. The Green's functions were computed assuming the 1D velocity model proposed Matsubara et al. (2008) for the studied area (Table 1).

Figure 2 shows the source model, in terms of final slip distribution on the fault plane, obtained by averaging a subset of nearly 300.000 rupture models from the whole model ensemble. The selected rupture histories correspond to those models having a cost function, in term of L2 norm of observed and simulated data, not exceeding the 5% of the misfit value corresponding to the best fitting model (Cirella et al., 2008). The rest of source kinematic parameters' distributions inferred from strong motion data inversion are shown in Figure S1 of Electronic Supplement.

The retrieved model is characterized by two principal patches of slip (Figure 2): a shallow small patch in the NE direction from the nucleation point, and a larger one extending SW from the hypocenter to the southern shallow part of the fault plane. The larger asperity is characterized by a peak slip-velocity of 4.0÷6.5 m/s, corresponding to a dislocation of about 3.5÷5.5 m, while the smaller one shows a peak slip-velocity of 3.5÷4.5 m/s, corresponding to 2.5÷3.5 m of slip. Both asperities are characterized by a rise time ranging between 2.5 and 3.5 s. The main features of the inferred slip distribution and the resulting seismic moment ($Mo = 3.65 \times 10^{19}$ Nm) fairly agree with the results found by Suzuki et al. (2010). The slip direction is consistent with a nearly pure reverse faulting mechanism (black arrows in Figure 2). The total rupture duration is about 11 s with a mean rupture velocity of about 1.8 km/s along strike and 2 km/s along the down-dip directions. The agreement between observed and synthetic data is in general satisfactory: the synthetic ground velocities match fairly well the recorded seismograms at most of the stations selected for the inversion analysis (Figure S2 in Electronic Supplement).

2.2 The reference shakemaps

Ground motion parameters (i.e., PGA, PGV, and spectral acceleration at 3s) inferred from seismograms recorded at 116 surface seismic stations (66 from K-NET, 50 from KiK-net) were used to compute shaking maps associated to the Iwate-Miyagi Nairiku event. The selected ground motion parameters describe the ground motion behavior in different frequency band covering the all range of interest (high frequency for PGA, intermediate for PGV and low for SA at 3s). The maps obtained are shown in Figure 3**.** These maps are referred hereafter as *Myiagi A* or simply reference maps, because they rely almost totally on the recorded motion and they are used as reference for all the tests.

We used the GMPE developed exclusively from Japanese data by Kanno et al. (2006) in order to include the regional characteristi**c**s of strong-motion attenuation in the ground motion estimates at the phantom points.

The site amplification effects have been accounted for through the Borcherdt (1994) coefficients. They are based on the Vs30 measured at each recording site, obtained from the K-NET and KiK-net databases or estimated from the topographic slope at the phantom points (Wald and Allen, 2007).

Finally, as proposed in several ShakeMap applications, a bias factor was computed by minimizing the difference between the observed ground-motion parameters at the recording sites within 70 km from the epicenter and the corresponding estimates from GMPEs. The predicted ground-motion parameters have been then multiplied by the bias factor to fit the recorded data for that event in order to overcome possible deficiencies related to magnitude determination and fault dimension estimation in the first minutes after the earthquake. The bias values, reported in Table 2, show that the bias effect is negligible for estimated PGAs and slightly negative for PGVs and PSAs (Figure 3b).

The comparison between the shakemaps computed for the different cases with respect to the reference ones allowed us to evaluate the improvement of the ground-motion prediction that was quantified in terms of maps of residuals, defined as:

$$RES = \log_{10}(Y_A) - \log_{10}(Y_X) \quad (1)$$

where Y is a strong motion parameter (PGA, PGV and PSA), the subscripts A refers to the reference shakemaps and X to the shakemaps computed using different sets of data. Residuals are calculated from ground motion values sampled on a regular grid of 1.5 km on the maps. The residual maps obtained in this way assess the error that ShakeMap would commit in the ground motion estimation. In fact, positive values of RES indicates an underestimation with respect to the reference map, whereas negative values of RES indicates an overestimation of the reference map. A more quantitative description of the differences between the shakemaps has been obtained looking at the distribution of residuals within 50 km from the epicenter, as we are mainly interested in near-fault ground motions estimation.

3. Shakemaps from GMPE ground motion estimates (Test 1)

The first test (Test 1) was devoted to study the shakemap improvement when using an increasing number (from 0% to 76%) of available recording stations. The five different subsets are chosen with different criteria, as detailed in Table 3, and are named adding the suffix 1 to recall the Test 1. In each case study, the missing recordings are indeed replaced with a simple evaluation of the ground motion obtained by suitable GMPEs, for which only some basic information (magnitude, fault geometry and hence distance from the fault) are necessary and can be inferred very soon after the earthquake occurrence.

We first evaluated the case (rare but still possible) of absence of recording stations in the study area (case B1, Table 3 and Figure 4). In this case all the ground motion parameters at the phantom points are computed using the GMPEs only. Note that it is not possible to define any bias value since, in this case, no data are available to compute it. The use of the GMPE without any real observations generates shakemaps overpredicting in general the reference maps (i.e., negative residuals in Figure 4), because the used GMPE predicts values higher than the actual recorded data (Figure 3b). The maps show also large positive residuals in a small area NW to the epicenter, which are due to the high PGA recorded at station AKTH04 (249 %g on the EW component); the recorded value exceed the GMPEs by 3 standard deviations and it is likely related to peculiar site effects. In this case the GMPE itself is not able to predict reliable ground motion values.

In Figure 5 we show the residuals maps for the other analyzed cases that are characterized by an increasing number of the recording stations (from 10% to 76% of the whole available dataset, Table 3). In the case C1 (Table 3 and Figure 5a) we considered only the surface data recorded at the 13 sites used for the source model inversion. In this case the shakemaps underestimate the reference

maps mostly close to the source, because the recorded values at the selected stations pull down the GMPE with an excessive bias value.

Increasing the number of sparse stations to 43% (case D1, Table 3 and Figure 5b) and then 76% (case E1, Table 3 and Figure 5c) of the total number of stations, the inter-station distances decrease to 17 km and 10 km, respectively. In these cases the ground motion evaluation improves significantly (Figure 5b and 5c), even though there is not a large difference between the two cases themselves.

Finally, we tested the ShakeMap capability to reproduce the ground motion in the near-source area when no recordings are available at epicentral distances lower than 50 km (case F1, Table 3 and Figure 5d). In this case the underestimation close to the fault becomes larger, particularly in the strike-normal direction. This performance is due to the bias effect, the GMPE being shifted using a larger bias because computed on data within 50 to 70 km range (in the case F all the stations are missing below 50km).

The previous tests allowed us to evaluate the error in shakemaps estimation when the station coverage is not as good as in the reference maps. As we are mainly interested in near-fault ground motion estimation, where the damage could be more severe, we quantified the variations within 50 km from the epicenter. Figure 6a shows the cumulative distributions of the residuals within 50 km from the epicenter for the different cases shown in the Figures 4 and 5. When no real records are available in the study area (case B1, Figure 4 and Figure 6a), almost 100% of the near-fault area presents negative residual values because the predicted values overestimate the real data. Increasing the number of recording stations, the median values move to the range 0-0.25 and the width of the distributions becomes narrow, that is the residuals vary between -0.1 and +0.5 (case C1-D1-E1, Figures 5 and 6a). The best performance for sites within 50 km from the epicenter is given by the case D1, where half of the stations are available, sparsely distributed on the whole area. Although a larger number of stations is removed in D1 with respect to F1 (66 and 28 stations removed, respectively), the shakemap is more accurate in D1 than in F1, because in the latter case all the stations within 50 km from the epicenter are missing (Figures 5 and 6a). This result remarks the importance of observations in the near-source area: shakemaps are more and more reliable as the coverage of stations near the earthquake source is dense and uniformly distributed.

4. Hybrid shakemaps from ground-motion simulation (Test 2)

In the second test (Test 2) we investigated whether ground motion parameters estimated from synthetic seismograms could improve the shakemaps when recorded data are scarce but information on seismic source are available. To this aim, we used the hybrid Deterministic-Stochastic Method (DSM), proposed by Pacor et al. (2005), which allows for simulating the ground motion caused by an extended fault. The method preserves the very simple nature of the stochastic model where only few parameters need to be specified in the ground-motion calculation (Boore, 2003), but it accounts

also for the rupture model parameters, such as the fault geometry, hypocenter position, rupture velocity and slip distribution. Such characteristics make the method suitable for the generation of near-fault synthetic seismograms when source rupture model is identified (Pacor et al., 2005; Ameri et al., 2008; Emolo et al., 2008; Cultrera et al., 2009; Ameri et al., 2009; Ameri et al., 2011).

The ground motions have been simulated at the 116 recording stations using the same 1D crustal structure adopted for the inversion of strong-motion data (Table 1). The simulations were computed at bedrock, and the ground motion parameters were afterwards multiplied by the site amplification factors proposed by Borcherdt (1994) and obtained as described in the section 2.2.

The attenuation model needed by DSM is reported in Table 4 and it is based on the work by Satoh et al. (1997). As source model we consider the solution obtained through the inversion of strong-motion data as described in section 2.1, assuming a focal mechanism 209/40/105. The adopted slip distribution (Figure 2) is characterized by a larger slip patch in the southern portion of the fault. The hypocenter is located approximately at the center of the fault at a depth of 6.5 km and the rupture front propagates with a constant rupture velocity of 1.8km/s, that corresponds to the mean value of the rupture velocity distribution inferred from the source inversion. Finally, we assumed an instantaneous rise-time for the source-time function. All these parameters can be quickly inferred after the earthquake occurrence and then they could be available in the immediate post-event for simulation studies.

First, we verified the accuracy of the simulations by checking the agreement between observed and simulated values at each recording site, both in terms of amplitude level and distance dependence (Figure 7, left panels). The fit is generally satisfactory despite the simple source and site parameterization adopted in the model. Some of the limitations of the simulation model are shown in the residuals maps of Figure 7 (right panels) where the complexity of site response in the large alluvial basins (i.e., the Sendai basin to the south) is not reproducible by the simple site amplification coefficients adopted in the simulation. Moreover, significant PGA (Figure 7a) and PGV (Figure 7b) underestimation occurs at two sites close to the fault (AKTH04 and MYG004) and at distances larger than about 60-70 km (mainly for PGA). The high observed PGAs in the north-east region are mainly located NE to the epicenter and are possibly related to crustal propagation effects (Spagnuolo, 2010, and Spagnuolo et al., 2010).

We then computed shakemaps using the simulated ground motion parameters at sites where the data are progressively removed from the reference dataset (Figure 8). The different scenarios are named as in Table 3 adding the suffix 2.

When only the 13 stations used for the source model characterization are available (case C2, Figure 8a), the shakemaps is based on a large number of synthetics. In this case the ground motion evaluation improves significantly with respect to case C1 (Figure 5a), where the missing recordings are replaced by GMPE estimates. In particular, the residual maps show good fits for distances smaller than 50km, while the PGA underestimation at larger distances, is due to the small peak values inferred from synthetics.

Increasing the number of recording stations (i.e., decreasing the number of simulated sites; case D2 and E2, Table 3) the fit with respect to the reference maps improves (Figures 8b and 8c), although the differences on the residual maps with respect to the cases D1 and E1 (Figure 5b and 5c) are not so large.

Finally, the use of synthetics allows us to improve the similarity with the reference shakemap, even in the case when the area within 50 km to the epicenter has not records available (case F2, Table 3). The improvement respect to F1 is due to the high bias value computed on data between 50 and 70 km only (stations are missing below 50km), which decreases when synthetics are included (case F2, Figure 8d).

A better quantitative view of the differences between the shakemaps can be obtained looking at the residual distribution within 50km to the epicenter (Figure 6). Figure 6b shows that there is an improvement for all the analyzed cases when using the hybrid shakemaps. The median values for PGV and PSA at 3s approach zero while median values for PGA residuals shown a small but systematic underestimation of reference shakemaps.

5. Application to Ms 6.9, 1980 Irpinia earthquake

Based on the results obtained for the 2008 Iwate-Miyagi Nairiku earthquake, we studied the Ms 6.9 1980 Irpinia (southern Italy) earthquake, a normal fault event with similar magnitude. The fault rupture was characterized by three different episodes occurring at 0s, 20s and 40s (Bernard and Zollo, 1989) and we computed the hybrid shakemaps for the 0s rupture, integrating the available data with DSM simulations.

Among the recordings of 21 analog accelerometric stations, we selected seven near-fault stations (within 60 km from the epicenter) that clearly recorded the 0 s event and were weakly affected by site effects (Ameri et al., 2011; strong motion data are available at the Internet Site for European Strong-Motion Data; Ambreseys et al., 2004). The density of the recording stations is similar to the case C of Iwate-Miyagi Nairiku earthquake (Table 3), for which we observed a remarkable improvement of the predicted motion using the hybrid shakemaps (Figure 5a and 7a).

We first computed the standard shakemaps by using the few records available and adopting the GMPEs proposed by Ambreseys et al. (1996) (Figure 9, left panels). We then integrated the available data with DSM ground motion simulations on a dense grid of virtual receivers radially distributed around the fault (Figure 9, central panels). All the synthetics are taken from Ameri et al. (2011), who performed a simulation study for this earthquake. For both computations (standard and hybrid ShakeMaps) the values are corrected for site effects by using the Vs30 inferred from the topography (see section 2.2), as described in Michelini et al. (2008).

Following the results obtained for the Iwate-Miyagi Nairiku earthquake (case C1 *versus* case C2), we assume that the hybrid ShakeMaps would improve the standard ones. The residual maps

between shakemaps with and without the synthetic values (Figure 9, right panels) show that the latter ones produce, in general, smaller values than expected by using the GMPE estimates. For this earthquake, the fault rupture propagated towards north-west and caused a back-directivity effect in the vicinity of the fault and to the south-east (Ameri et al., 2011).

The predicted PGV has been converted to the Mercalli–Cancani–Sieberg (MCS) intensity values using the Faenza and Michelini (2010) relation, and then compared with the MCS Intensity data-set from the Italian database of macroseismic information, DBMI04 (Stucchi et al. 2007). Figure 10 shows the macroseimic intensity shakemaps obtained with the standard ShakeMap procedure or integrated with the synthetics (hybrid shakemap). They are compared with the observed MCS intensity values (figure 10c), interpolated through a routine included in the Generic Mapping Tools package (Wessel and Smith, 1991). If we look at the higher intensity degrees, it is clear that the intensity field derived from the PGVs from the standard ShakeMap (figure 10a) cover an area larger than that was observed. In this case, the use of a GMPE produce a clear overestimation of the instrumental MCS intensities. On the other hand, the use of PGVs inferred from synthetic seismograms (figure 10b), defines an intensity areal distribution more similar to the observations (figure 10c). In the case of the 1980 Irpinia earthquake we have a poorly instrumented seismic event but the use of synthetics for the ShakeMap computation allows to better reproduce the heterogeneity of the felt shaking both in the vicinity of the fault and at regional scale.

6. Discussion and Conclusions

The main purpose of the ShakeMap package is to provide maps for post-earthquake response. However, possible lack of data in the epicentral area produces relevant uncertainties in the ground-motion distribution. To overcome these limitation, in this paper we investigated the shakemap improvement obtained by including ground-motion estimates from reliable synthetic seismograms instead of predictions from GMPEs, at sites where recordings are not available. Using the 2008, Mw 7.0, Iwate-Miyagi Nairiku (Japan) earthquake as case study, we computed the shakemaps for different distributions of recording stations by including the GMPE values at the phantom sites (Test 1) or the synthetic ground-motion values at new sites (Test 2).

We summarize the results within 50 km from the epicenter because we are interested in the near-fault ground motion estimation, where the highest shaking is expected. Table 5 reports the percentage of grid points where the predicted ground motion parameters range within 0.8 to 1.26 times the corresponding values in the reference maps (residuals within ± 0.1 for all the considered cases). The first test (Test 1), devoted to study the shakemap improvement when using an increasing number of available recording stations, remarks the importance of observations in the near-source area (Table 5): the shakemaps are more and more reliable as the coverage of stations near the earthquake source is dense and uniformly distributed (case D1).

The second test (Test 2) includes the DSM simulations in the ShakeMap computation. In general, the synthetics account for propagation and source properties in a more correct way than GMPE, and largely improves the results reaching good fitting levels regardless the density of the simulated stations: the difference between cases is not very large, and the percentage of grid points with small residuals (e.g., absolute value smaller than 0.1) is higher than 80% in almost all the cases (Table 5). In particular, the fit improves of about 10% for D2 and E2. When recordings are missing within 50 km from the fault (case F), the estimation through the GMPE (F1) is very poor in reproducing the reference map; however, when simulated values are included (case F2), the percentage of grid points with small residuals increases from 40-50% to 70-80%. The improvement is even more evident when very few recording stations are available (case C).

We extended the results obtained for the 2008, Mw 7.0, Iwate-Miyagi Nairiku earthquake to an event of similar magnitude and for which only few recording stations were available: the Ms 6.9, 1980 Irpinia (Southern Italy) earthquake. The hybrid shakemaps obtained integrating data with DSM synthetics indicate a distribution different from what expected by the standard shakemap, changing the peak distribution in the vicinity of the fault and lowering the ground motion especially south-east of the fault. The MCS intensity computed from PGV is consistent with the MCS intensity distribution inferred at the time of the earthquake.

This study encourage the use of extended source simulations in the framework of the ShakeMap implementations as already suggested by other authors (e.g. Moratto and Saraò, 2011). However, the rapid release of a shakemap requires a number of assumptions and simplifications that drives the choice of the input parameters and simulation methods. The DSM technique (Pacor et al., 2005) is, for instance, well suited to provide rapid estimates of ground motions including finite-fault effects. It demands few and easily available input data describing the earthquake source and the propagation medium (see section 4) and it runs in few minutes. The main features of the source (focal mechanism and geometry) can be obtained shortly after an earthquake from regional or teleseismic data and, within few hours, it is possible to have a detailed rupture model through the inversion of strong-motion data like the one we used to model the source of the Iwate-Miyagi earthquake. However, in DSM the source is defined by the focal mechanism, source geometry and a rough rupture model (estimate of the average rupture velocity and large-scale distribution of the slip patches). The crustal velocity model can be precompiled for different regions in order to be accessible in real time. Alternatively, pre-calculated either analytical or empirical Green's functions could be used to speed-up the source inversion and the ground-motion simulation in the proposed approach.

Full-wavefield deterministic methods (discrete-wavenumber, finite-element or finite-difference codes) could be also used, but they might face several problems for the quasi real-time applications: the numerical solution of the equation of motions is computationally expensive and can require from hours to days of computation time. Moreover such methods require an accurate knowledge of the propagation medium, often not available and, as a consequence, their application is currently restricted to the calculation of the low-to-intermediate frequency wavefield and they are not suitable for broadband ground-motion estimates.

Nowadays the generation of synthetic data is not implemented in the ShakeMap procedure for real-time applications, but some effort can be done to generate hybrid shakemaps at elapsed time, largely improving the predictions in the near source region when few recordings are available. The use of GMPE is still valid for a quick evaluation of a first order ground motion distribution, provided that the coverage of stations near the earthquake source is dense and uniformly distributed.

DATA and RESOURCES

Data related to the 2008, Mw 7.0, Iwate-Miyagi Nairiku earthquake have been downloaded from the K-NET (www.k-net.bosai.go.jp) and KiK-net (www.kik.bosai.go.jp*)* web sites maintained by the Strong Motion Seismograph Network Laboratory, Earthquake and Volcano Data Center, National Research Institute for Earth Science and Disaster Prevention 3-1, Tennodai, Tsukuba, Ibaraki 305-0006, Japan.

The 1980 Irpinia earthquake accelerometric data have been downloaded from the Internet Site for European Strong-Motion Data (http://www.isesd.hi.is), whereas the MCS Intensity data are available at http://emidius.mi.ingv.it/DBMI04/, with a revised release 1900–2008 (i.e. DBMI08)

The Generic Mapping Tools (Wessel and Smith, 1991) software package has been used to generate some figures.

ACKNOWLEDGEMENTS

We thank Licia Faenza, Elena Spagnuolo, André Herrero, Francesca Pacor and Alessio Piatanesi, for the fruitful discussions during the development of this study.

This research has benefited from funding provided by the Italian Presidenza del Consiglio dei Ministri – Dipartimento della Protezione Civile (DPC) under the contract 2007–2009 DPC-S3. Scientific papers funded by DPC do not represent its official opinion and policies. Antonella Cirella was supported by the FIRB-MIUR (RB1N047WCL) and the NERA-EC (262330) projects.

REFERENCES

Ambraseys, N.N., K.A. Simpson, J.J. Bommer (1996). Prediction of horizontal response spectra in Europe. Earthquake Engineering and Structural Dynamics 25 (4), 371–400.

Ambraseys N.N., P. Smit, J. Douglas, B. Margaris, R. Sigbjornsson, S. Olafsson, P. Suhadolc G. Costa, (2004). Internet site for European strong-motion data. Boll Geof Teor Appl 45(3): 113–129

Ameri, G., F. Pacor, G. Cultrera, G. Franceschina (2008). Deterministic ground-motion scenarios for engineering applications: The case of Thessaloniki, Greece, Bull. Seismol. Soc. Am. 98, 1289–1303.

Ameri, G., F. Gallovič, F. Pacor, A. Emolo, (2009). Uncertainties in strong ground-motion prediction with finite-fault synthetic seismograms: An application to the 1984 M 5.7 Gubbio, central Italy, earthquake, Bull. Seismol. Soc. Am. 99, 647–663.

Ameri G., A. Emolo, F. Pacor, F. Gallovič, (2011). Ground-Motion Simulations for the 1980 M 6.9 Irpinia Earthquake (Southern Italy) and Scenario Events. Bull .Seism. Soc. Am., 101, 3, 1136–1151; doi: 10.1785/0120100231

Bernard, P., and A. Zollo, (1989). The Irpinia (Italy) 1980 earthquake: detailed analysis of a complex normal faulting, J. Geophys. Res. 94, 1631–1647.

Boore, D. M., (2003). Simulation of ground motion using the stochastic method, Pure Appl. Geophys. 160, 635–676.

Borcherdt R. D., (1994). Estimates of Site-Dependent Response Spsectra for Design (Methodology and Justification), Earthquake Spectra 10, 617.

Bragato P.L., P. Di Bartolomeo, D. Pesaresi D.,M.P. Plasencia Linares and A. Saraò, (2011). Acquiring, archiving, analyzing and exchanging seismic data in real time at the Seismological Research Center of the OGS in Italy. Annals Geophysics, 54, 67-75; doi: 10.4401/ag-4958.

Cirella A., A. Piatanesi, E. Tinti, M. Cocco, (2008). Rupture process of the 2007 Niigata-ken Chuetsu-oki earthquake by non-linear joint inversion of Strong Motion and GPS data" Geophys. Res. Lett., 35, L16306, doi:10.1029/2008GL034756.

Convertito V., M. Caccavale, R. De Matteis, A. Emolo, D. Wald, A. Zollo, (2011). Fault extent estimation for near-real time ground shaking map computation purposes. Accepted for publication on Bull. Seism. Soc. Am.

Cultrera G., F. Pacor, G. Franceschina, A. Emolo., M. Cocco, (2009). Directivity effects for moderate-magnitude earthquakes (Mw 5.6–6.0) during the 2 1997 Umbria–Marche sequence, central Italy. Tectonophysics 476 (2009), pp. 110-120, DOI information: 10.1016/j.tecto.2008.09.022

Dreger, D.S., L. Gee, P., Lombard, M.H. Murray, B. Romanowicz, (2005). Rapid finite-source analysis and near-fault strong ground motions: application to the 2003 Mw 6.5 San Simeon and 2004 Mw 6.0 Parkfield earthquakes, Seism. Res. Lett., 76(1), 40–48.

Emolo A., G. Cultrera, G. Franceschina, F. Pacor, V. Convertito, M. Cocco, A. Zollo, (2008). Ground motion scenarios for the 1997 Colfiorito, central Italy, earthquake. Ann. Geophys. 51, 509-525.

Emolo A., V. Convertito, L. Cantore, (2011). Ground-motion predictive equations for low-magnitude earthquakes in the Campania–Lucania area, Southern Italy. J. Geophys. Eng., 8, 46–60, DOI:10.1088/1742-2132/8/1/007.

Faenza L. and A. Michelini, (2010). Regression analysis of MCS intensity and ground motion parameters in Italy and its application in ShakeMap, Geophys. J. Int. (2010) 180, 1138–1152

Faenza L., V. Lauciani, A. Michelini, (2011). Rapid determination of the shakemaps for the L'Aquila main shock: a critical analysis. Bollettino di Geofisica Teorica ed Applicata Vol. 52, n. 3; 407-425, September 2011, DOI 10.4430/bgta0020

Fukushima Y., J.C. Gariel, R. Tanaka, (1995). Site-dependent attenuation relations of seismic motion parameters at depth using borehole data Bull. Seism. Soc. Am., 85, 1790 - 1804.

Iannaccone G., A. Zollo, L. Elia, V. Convertito, C. Satriano, C. Martino, G. Festa, M. Lancieri, A. Bobbio, T.A. Stabile, M. Vassallo, A. Emolo, (2010). A prototype system for earthquake early-warning and alert management in southern Italy. Bull. Earthquake Eng., 8, 1105–1129, DOI: 10.1007/s10518-009-9131-8.

Kanno T., A. Narita, N. Morikawa, H. Fujiwara and Y. Fukushima, (2006). A New Attenuation Relation for Strong Ground Motion in Japan Based on Recorded Data. Bull. Seism. Soc. Am., 96, 879-897; DOI: 10.1785/0120050138.

Kato, K., M. Takemura, T. Ikeura, K. Urao, T. Uetake, (1992). Preliminary analysis for evaluation of local site effects from strong motion spectra by an inversion method, J. Phys. Earth 40, 175–191

Matsubara M., K. Obara, K. Kasahara, (2008). Three-dimensional P- and S-wave velocity structures beneath the Japan Islands obtained by high-density seismic stations by seismic tomography. Tectonophysics, 454, 86-103; doi:10.1016/j.tecto.2008.04.016.

Michelini, A., L. Faenza, V. Lauciani, L. Malagnini, (2008). ShakeMap implementation in Italy. Seism. Res. Lett., 79, 688–697.

Moratto, L., G. Costa, P. Suhadolc, (2009). Real-time generation of ShakeMaps in the Southeastern Alps. *Bull. Seismol. Soc. Am.,* **99**, 2489–2501.

Moratto L. and A. Saraò (2011). Improving ShakeMap performance by integrating real with synthetic data: tests on the 2009 M_w=6.3 L'Aquila earthquake (Italy). Submitted to J. Seism.

Pacor F., G. Cultrera, A. Mendez, M.Cocco (2005). Finite Fault Modeling of Strong Ground Motions Using a Hybrid Deterministic–Stochastic Approach. Bull. Seism. Soc. Am., 95, 1, 225-240.

Piatanesi A., A. Cirella, P. Spudich, M. Cocco, (2007). A global search inversion for earthquake kinematic rupture history: Application to the 2000 western Tottori, Japan earthquake. J. Geophys. Res., 112, B07314, doi:10.1029/2006JB004821.

Rhie, J., D.S. Dreger, M. Murray, N. Houlié, (2009). Peak ground velocity ShakeMaps derived from geodetic slip models. Geophys. J. Int., 179, 1105–1112, doi: 10.1111/j.1365-246X.2009.04327.x

Satoh T., H. Kawase, T. Sato, (1997). Statistical spectral model of earthquakes in the eastern Tohoku district, Japan, based on the surface and borehole records observed in Sendai, Bull. Seism. Soc. Am., 87, 446 - 462.

Spagnuolo E., (2010). Fault Directivity and Seismic Hazard. PhD Thesis in Geophisics, Università degli Studi di Genova, Scuola di dottorato in meccanica dei fluidi e dei solidi, XXII ciclo 2007-09.

Spagnuolo E., L. Faenza, G. Cultrera, A. Michelini, A. Herrero, A. Saraò, (2010). Accounting for Rupture Directivity in ShakeMap. SD3/P7/ID46. European Seismological Commission 32nd Genearl Assembly, Sept 6-10 2010, Montpellier, France. http://www.esc2010.eu/cd/search/poster/n0326_SD3_P7_ID46_Spagnuolo_E.html

Spudich, P. and B. S. Chiou, (2008). Directivity in NGA Earthquake Ground Motions: Analysis Using Isochrone Theory. Earthquake Spectra 24(1), 279-298.

Stucchi, M., et al., (2007). DBMI04, il database delle osservazioni macrosismiche dei terremoti italiani utilizzate per la compilazione del catalogo parametrico CPTI04., Quaderni di Geofisica, 49, http://portale.ingv.it/produzione-scientifica/quaderni-di-geofisica/archivio/resolveUid/0c549ba6165e5d96636aba24f3677c17.

Suzuki, W., S. Aoi, H. Sekiguchi, (2010). Rupture Process of the 2008 Iwate–Miyagi Nairiku, Japan, Earthquake Derived from Near-Source Strong-Motion Records. Bull. Seismol. Soc. Am., 100(1), 256-266, doi:10.1785/ 0120090043.

Wald D.J., V. Quitoriano, T.H. Heaton, H. Kanamori, C.W. Scrivner, C.B. Worden, (1999). TriNet "ShakeMaps": Rapid generation of peak ground motion and intensity maps for earthquakes in Southern California. Earthq. Spectra. 15, 537-555.

Wald D.J. and T.I. Allen, (2007). Topographic slope as a proxy for seismic site conditions and amplification. Bull Seismol Soc Am 97(5):1379–1395. doi:10.1785/0120060267

Wessel P. and W. H. F. Smith, (1991), Free Software Helps Map and Display Data. EOS Trans. AGU, 72, p441, 445-446

TABLES

Table 1. The 1-D crustal velocity model used in this study (after Matsubara et al., 2008). P-wave velocity (Vp) in the upper 3 layers is diminished of 10% respect to their original values, to account for the mismatch delay of the P arrivals. S-wave velocity (Vs) is computed as Vp/√3.

Depth (km)	Vp (km/s)	Vs (km/s)	Density (g/cm^3):
0.0	4.8	2.7	2.60
2.0	5.1	2.9	2.65
4.0	5.3	3.0	2.70
14.0	6.4	3.6	2.80
25.0	6.8	3.9	2.83
27.0	7.0	4.0	2.90
30.0	7.2	4.1	3.00
266.	8.5	4.8	3.40

Table 2. Bias values for the reference map. Negative values indicate that the adopted GMPE provides, on average, values higher than observed motions and thus they will be shifted to smaller values in the ShakeMap procedure. Analogous comments apply to positive bias values. See the text for bias definition and determination.

PGA	PGV	PSA(0.3s)	PSA(1s)	PSA(3s)
0.00	-0.22	-0.11	-0.60	-0.14

Table 3. Case studies corresponding to different subsets of recording stations investigated in Test1 and Test2. The original dataset used to compute the reference shakemaps consists of 116 stations.

CASE	RECORDS USED		REMARKS
B	0	0 %	No recorded data are used. Shakemaps rely only on GMPEs
C	13	10%	Only the stations selected for inverting the source model
D	50	43%	Only KiK-net stations
E	81	70%	Removed 35 K-NET stations deployed on site classes A and B
F	88	76%	Only stations at epicentral distances larger than 50 km are considered

Table 4. Ground-motion attenuation parameters for DSM simulation technique: geometrical spreading G(R), being R the source-to-receiver distance, anelastic attenuation function Q(f), being f the frequency, and high-frequency decay parameter f_{max}. These values have been proposed by Satoh et al. (1997) who used strong motion records from 18 earthquakes ($3.4 \leq M_{JMA} \leq 7.1$) occurred in the eastern Tohoku district (including Iwate, Miyagi and Fukushima prefectures) to derive a spectral model valid for the area.

parameter	**function**	**comments**
G(R)	1/R	most of the earthquake considered by Satoh et al. (1997) are subduction events; for shallow crustal events the geometrical spreading may depart from this behavior
Q(f)	$110\ f^{0.69}$	this choice is also consistent with results found by Fukushima et al. (1995) and Kato et al. (1992)
f_{max}	13.5 Hz	the maximum frequency has almost no dependency on seismic moment

Table 5- Percentage of grid points within 50 km from the epicenter and whose ground motion parameters are within 0.8 to 1.26 times the corresponding values in the reference map (residuals in the range [-0.1,0.1]). Shakemaps are computed (1) using different subset of recording stations (Test 1) and (2) integrating the missing data with DSM synthetics (Test 2).

	C1	C2	D1	D2	E1	E2	F1	F2
PGA	55%	75%	92%	94%	84%	94%	39%	77%
PGV	36%	81%	87%	96%	90%	98%	66%	81%
PSA(3s)	15%	77%	74%	82%	81%	90%	42%	70%

FIGURES

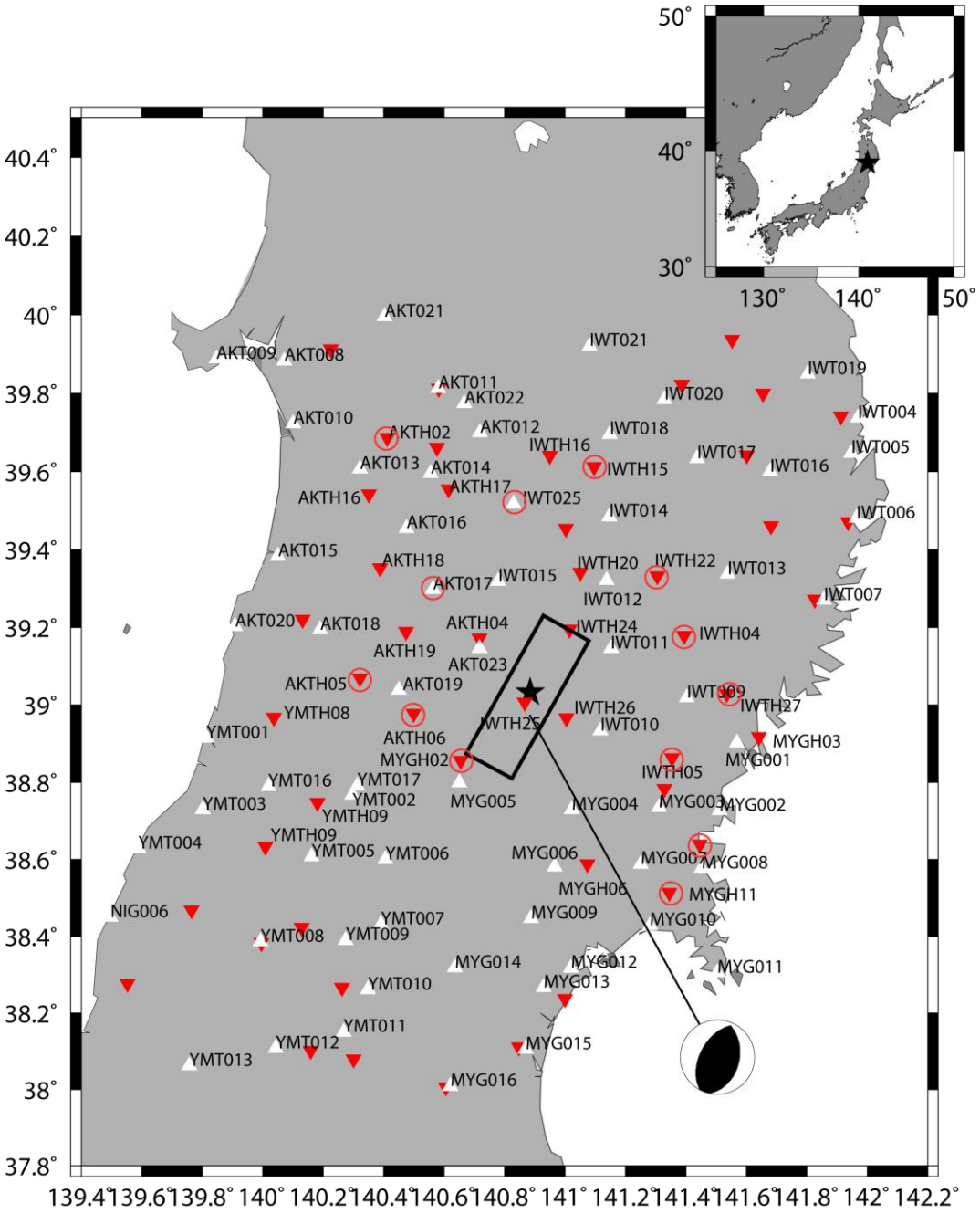

Figure 1. Map with location of K-NET (white) and KiK-net (red) accelerometric stations selected for this study. The black star indicates the epicenter of the 2008, Mw 7.0, Iwate-Miyagi Nairiku (Japan) earthquake. The focal mechanism after Suzuki et al. (2010) is also shown. Circles represent the K-NET and KiK-net strong motion stations whose records were inverted to infer the source kinematic characteristics. The black box represents the surface projection of the fault plane adopted in this study.

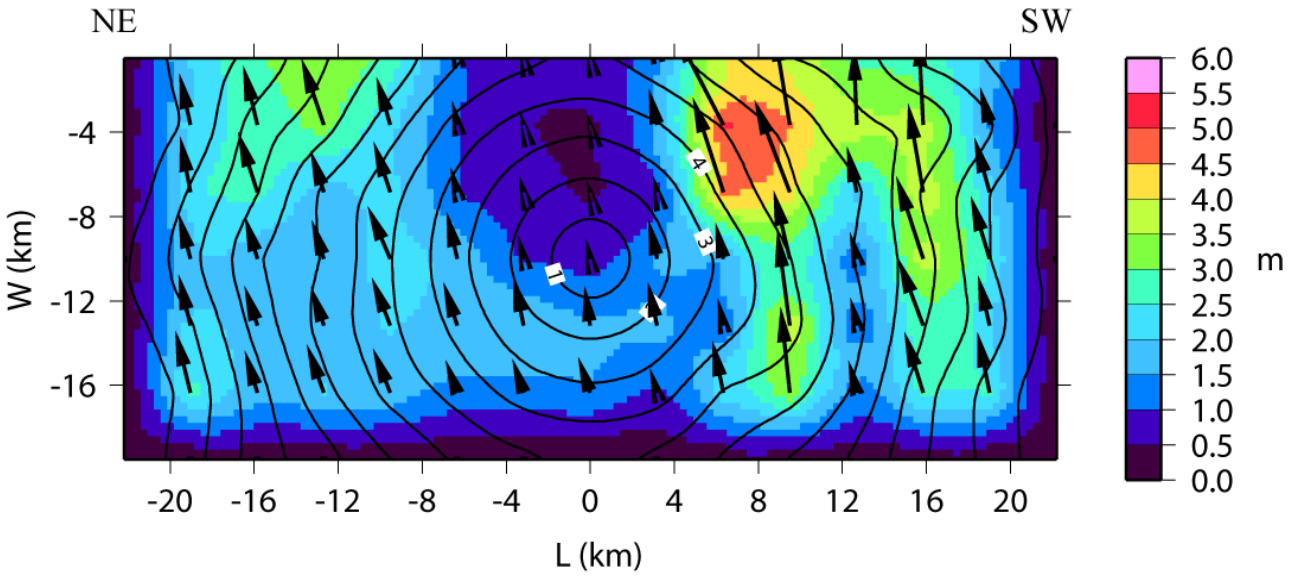

Figure 2. Rupture model for the 2008 Iwate-Miyagi Nairiku earthquake determined from the inversion of strong motion data recorded at stations indicated as circles in figure 1. Color scale refers to the final slip distribution, rupture times are shown by black contour lines (in seconds) while black arrows represent the slip vector. The nucleation point is located about 22.2 km along the strike and 10 km down-dip, from the upper left corner of the fault plane. The mean values of the final slip is about 1.95 m.

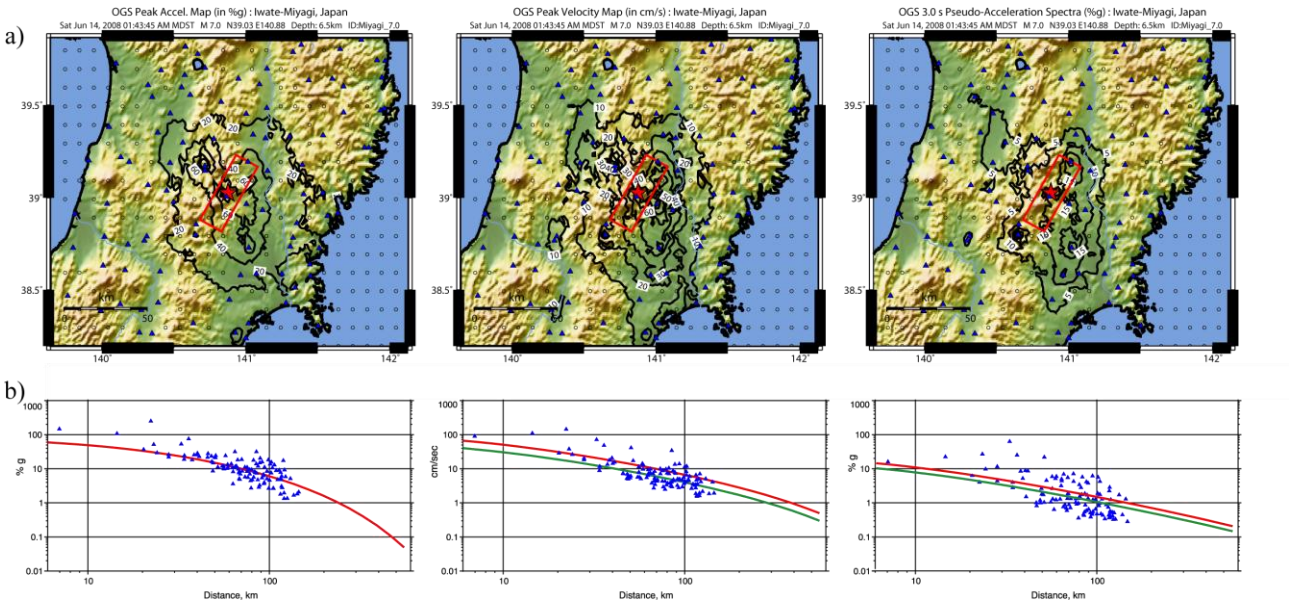

Figure 3. Distribution of PGA, PGV and PSA at 3 s: (a) reference shaking maps for the Iwate-Miyagi Nairiku earthquake obtained using all the recorded data (denoted as Myiagi A shakemaps); the red rectangles represent the surface fault projection while the red star is the earthquake epicenter; (b) recordings (triangles) and Kanno et al. (2006) predictive equation (solid red line) as a function of rupture distance (R_{CD}). The median GMPE (green solid line; Table 2) is scaled according to the bias values (see text for details).

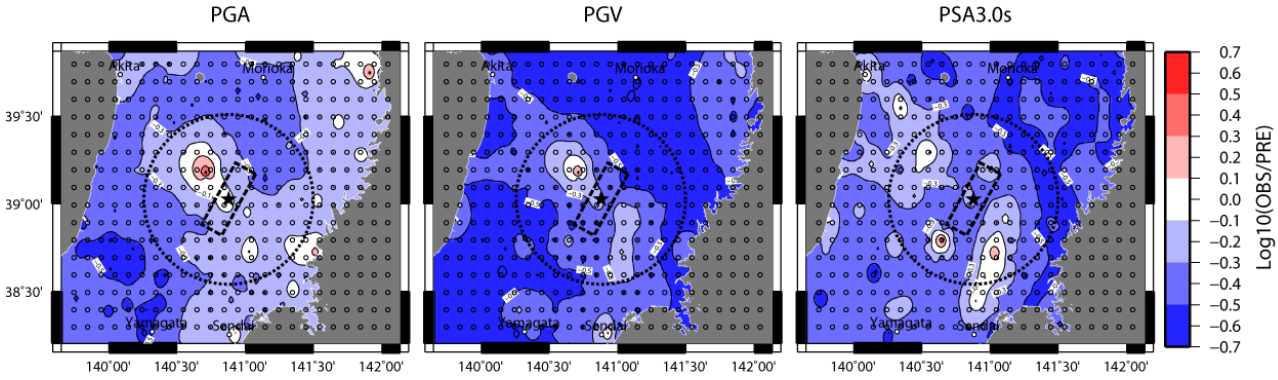

Figure 4. Maps of residuals (as defined in the equation 1) when recorded data are not considered (case B1, table3) for PGA, PGV and PSA at 3s. The black circle encloses grid points within 50 km from the epicenter.

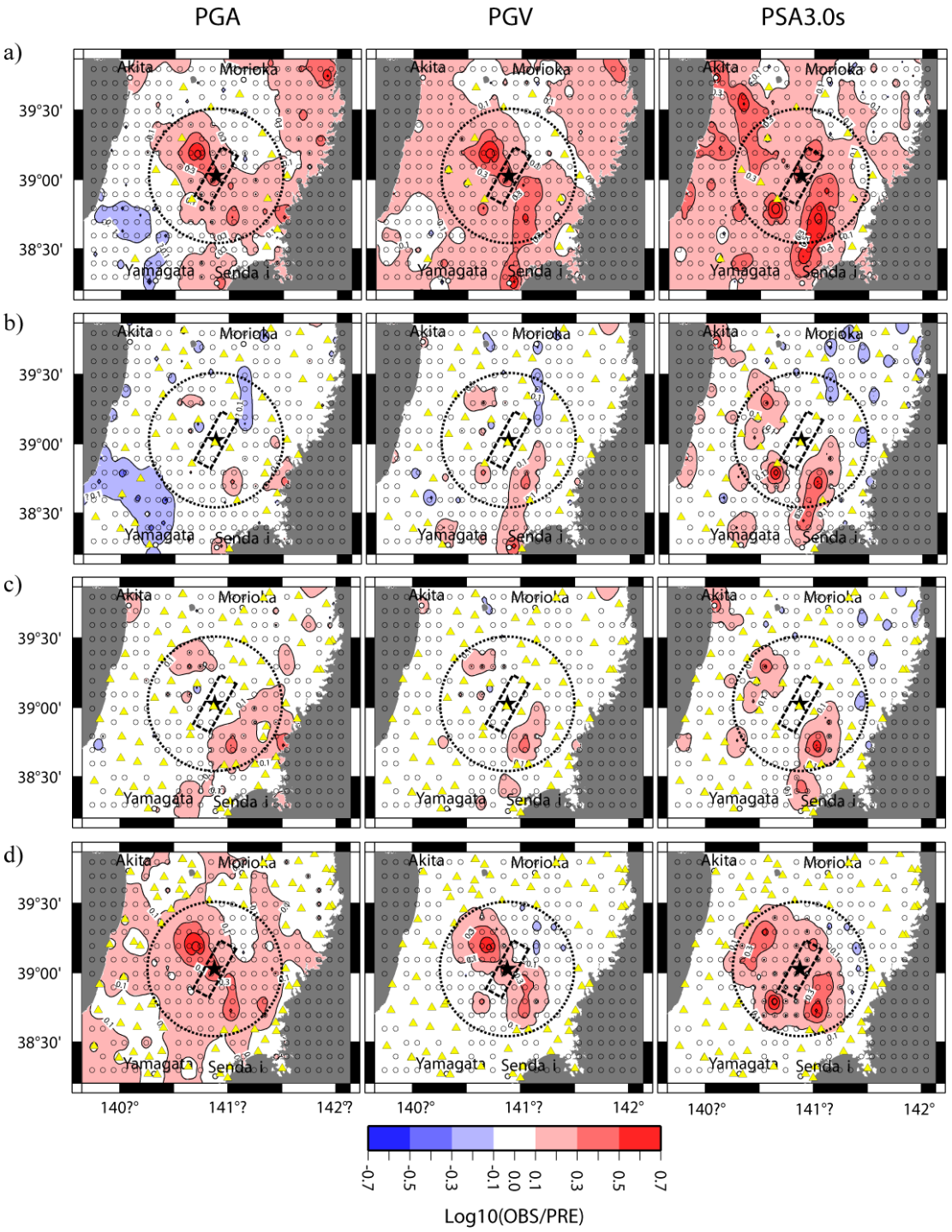

Figure 5. Residuals (as defined in the equation 1) maps for PGA, PGV and PSA at 3s using different subset of recording stations (Table 3, Test 1): (a) case C1 (10% of real data); (b) case D1 (43% of real data); (c) case E1 (70% of real data); (d) case F1 (76% of real data with epicentral distances larger than 50km). Yellow triangles and empty circles represent the recording stations and phantom points used in each case, respectively.

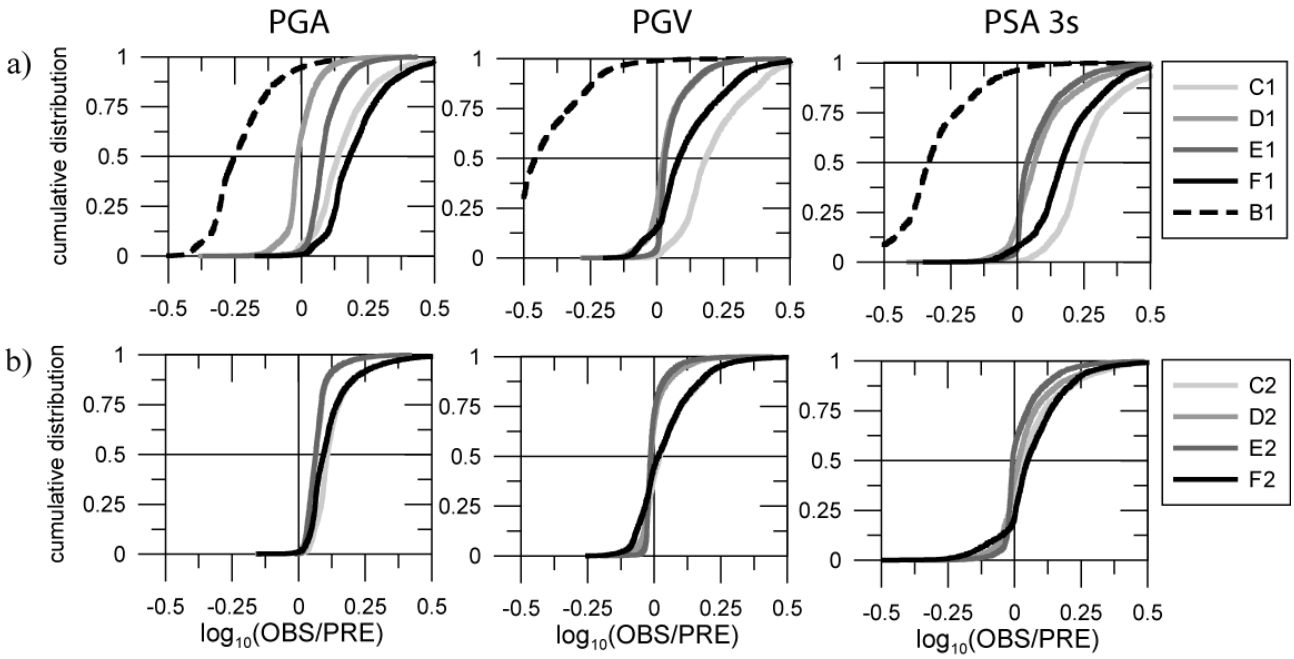

Figure 6. Cumulative distributions of residuals for PGA, PGV and PSA at 3s computed at grid points within 50 km from the epicenter (black circles in Figures 4-5-8). Plots refer to the two tests where we replaced the missing recordings with: (a) ground motion estimates from GMPEs (Test 1); (b) synthetic seismograms (Test 2). The legend refers to different subset of recording stations (Table 3): case B (recorded data are not available); case C (10% of real recordings); case D (43% of real recordings); case E (70% of real recordings); case F (76% of real recordings with epicentral distances larger than 50km).

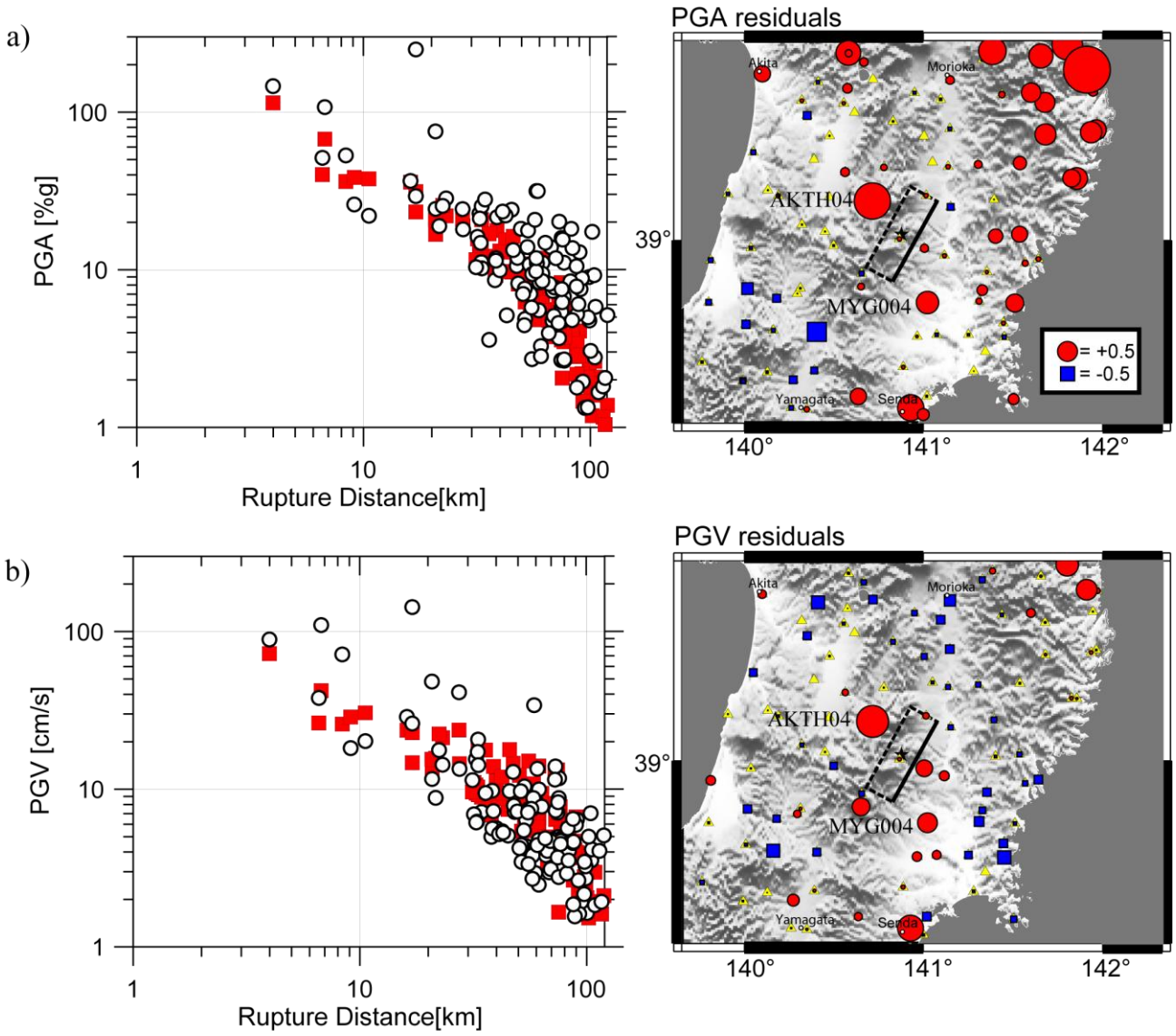

Figure 7. Left panels: comparison between recorded (white dots) and DSM simulated (red squares) (a) PGA and (b) PGV values (maximum from the two horizontal components) at the 116 recording sites, as a function of rupture distance. Right panels: maps of (a) PGA and (b) PGV residuals ($\log_{10}$(OBS/PRE)). Red circles and blue squares represent underestimation and overestimation of observed values, respectively. The dimension of symbol is proportional to the absolute value of the logarithm.

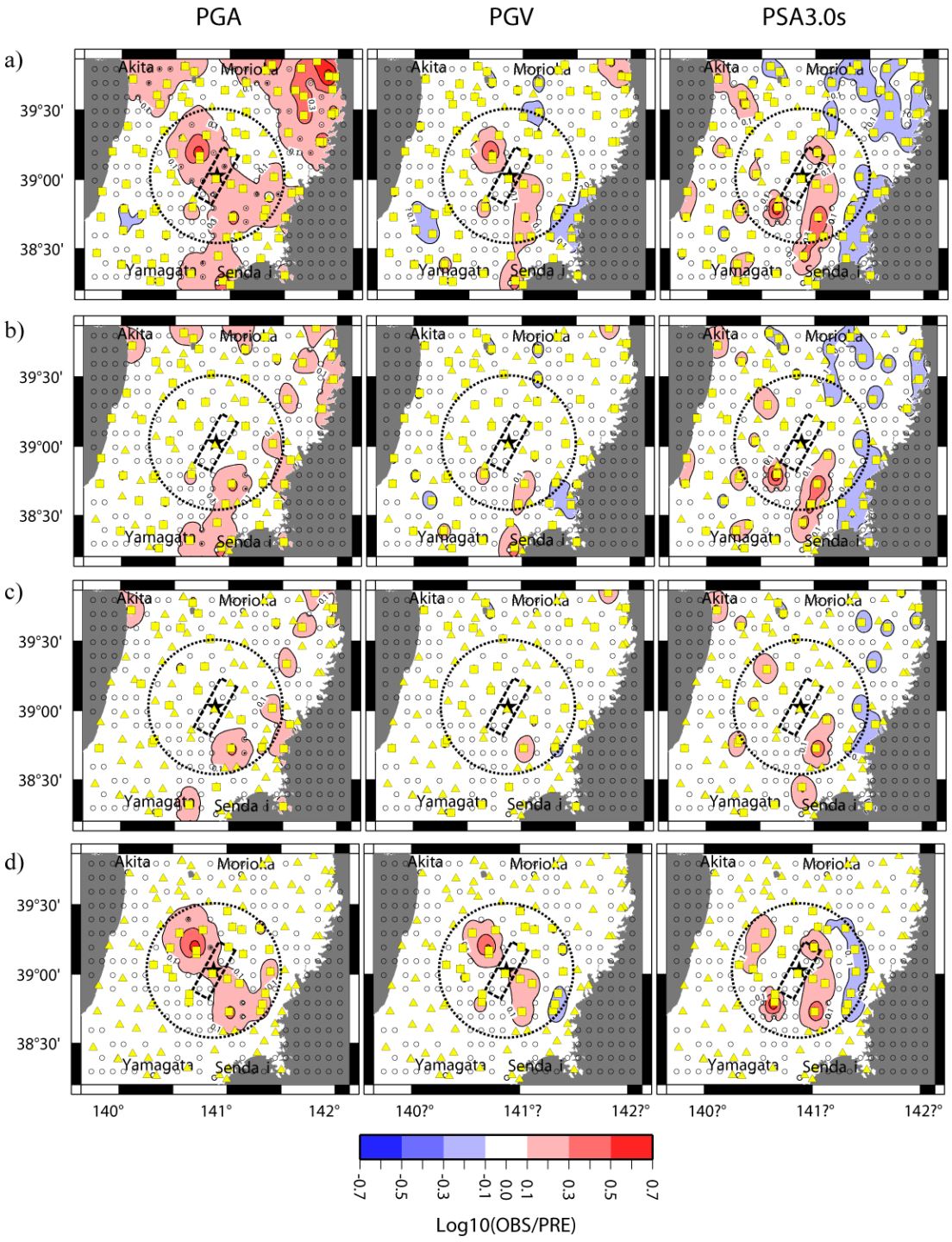

Figure 8. Maps of residuals (as defined in the equation 1) for PGA, PGV and PSA at 3s using different subsets of recording stations (Table 3), being the missing data substituted by synthetics (Test 2): (a) case C2 (10% of real data); (b) case D2 (43% of real data); (c) case E2 (70% of real data); case F2 (76% of real data with epicentral distances larger than 50km). Yellow triangles and squares represent the recording stations and the synthetic values, respectively, while empty circles are the phantom points.

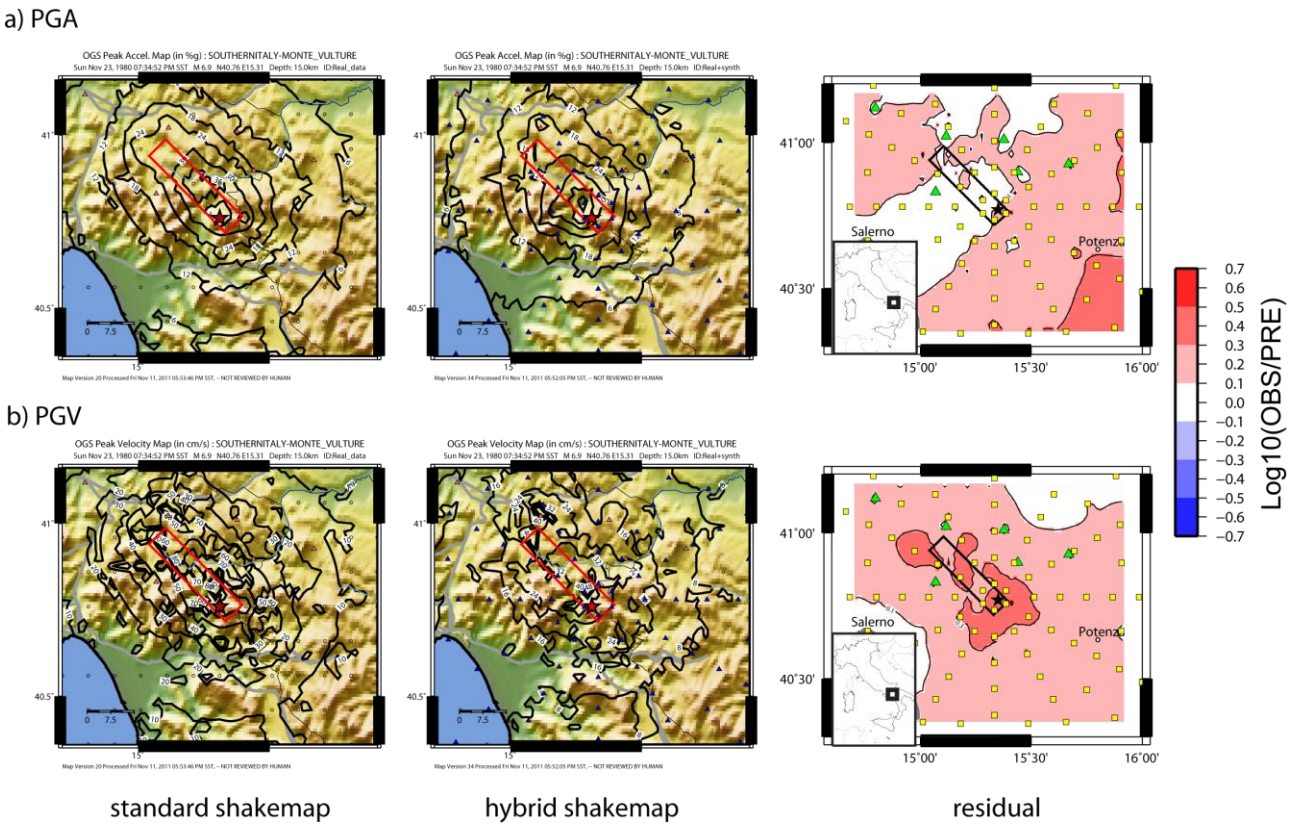

Figure 9. (a) PGA and (b) PGV values estimated for the 1980 Irpinia earthquake. Left panels: standard shakemaps. Central panels: hybrid shakemap with DSM simulations. Right panels: residual maps for the 1980 Irpinia earthquake; green triangles, yellow squares and empty circles represent the recording stations, synthetic values and phantom points, respectively.

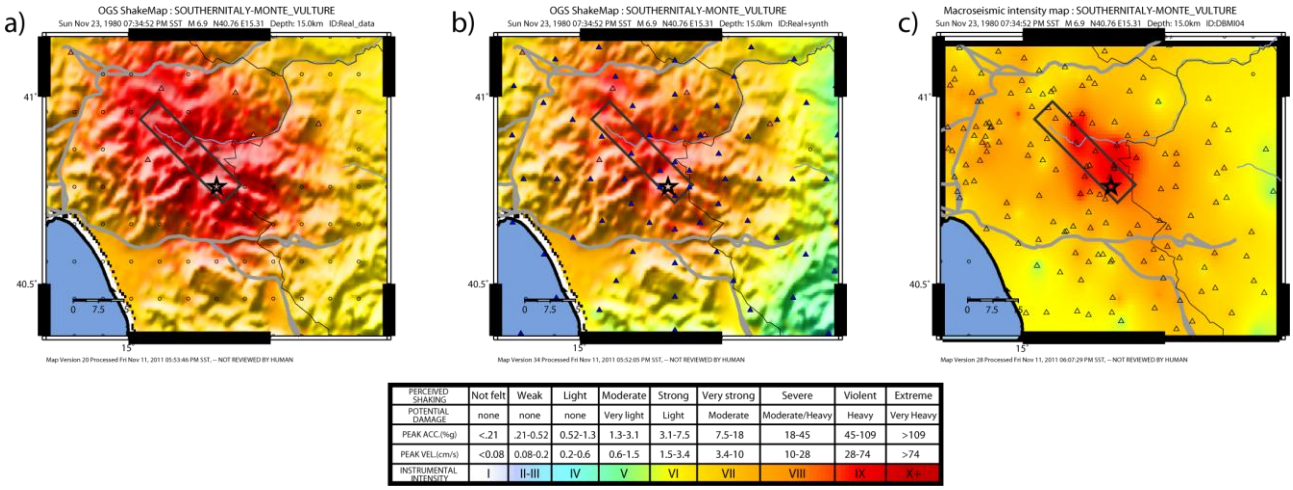

Figure 10. MCS intensity maps from: (a) PGV obtained with the standard ShakeMap procedure; (b) PGV obtained including synthetic data (hybrid ShakeMap); (c) observed values from DBMI04 database (Stucchi et al. 2007) interpolated with a GMT (Wessel and Smith, 1991) routine. The regression relation between intensities and PGV is from Faenza and Michelini (2010).

SUPPORTING INFORMATION

We display the results of the non-linear kinematic inversion technique (Piatanesi et al., 2007; Cirella et al., 2008) to image the source process on the fault plane for the Mw 7.0 Iwate-Miyagi Nairiku earthquake on June 13, 2008 (section 2 of this paper). Figure S1 show the plots of final slip, rise-time and peak slip-velocity distributions, together with the rupture time contour and the slip direction. The synthetic ground velocities are compared with the recorded seismograms in Figure S2.

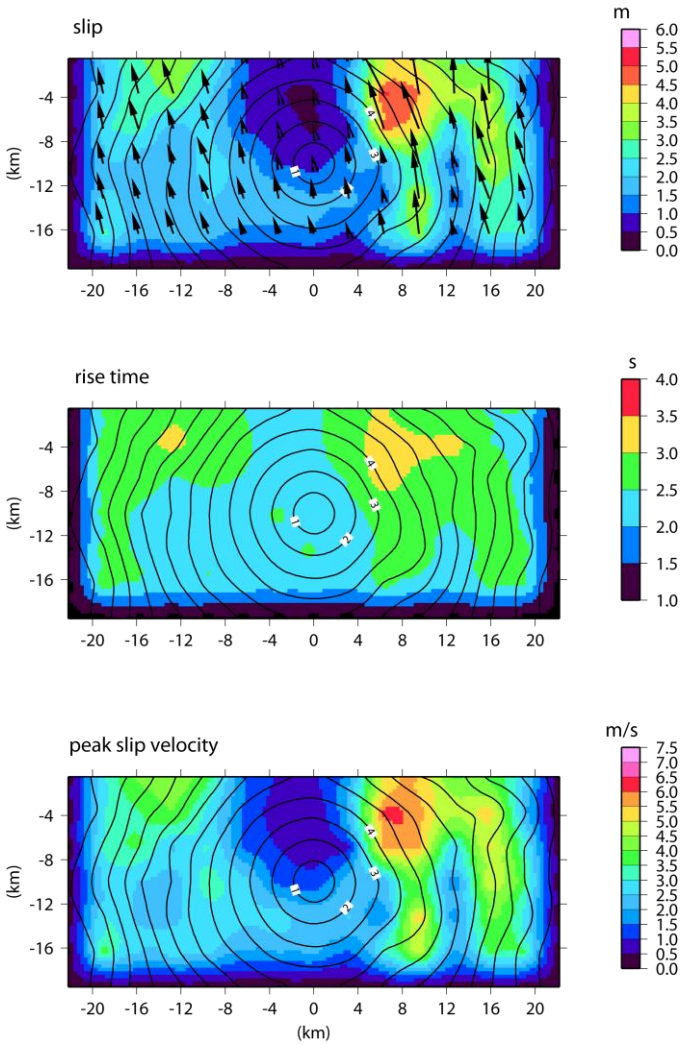

Figure S1. Rupture model for the 2008 Iwate-Miyagi Nairiku earthquake determined from the inversion of strong motion data recorded at a selected subset of data that recorded the earthquake, trough the technique proposed by Piatanesi et al. (2007). Upper, middle and bottom panels show final slip, rise-time and peak slip-velocity distributions, respectively. Rupture times are shown by black contour lines (in seconds) while black arrows displayed in upper panel represent the slip vector.

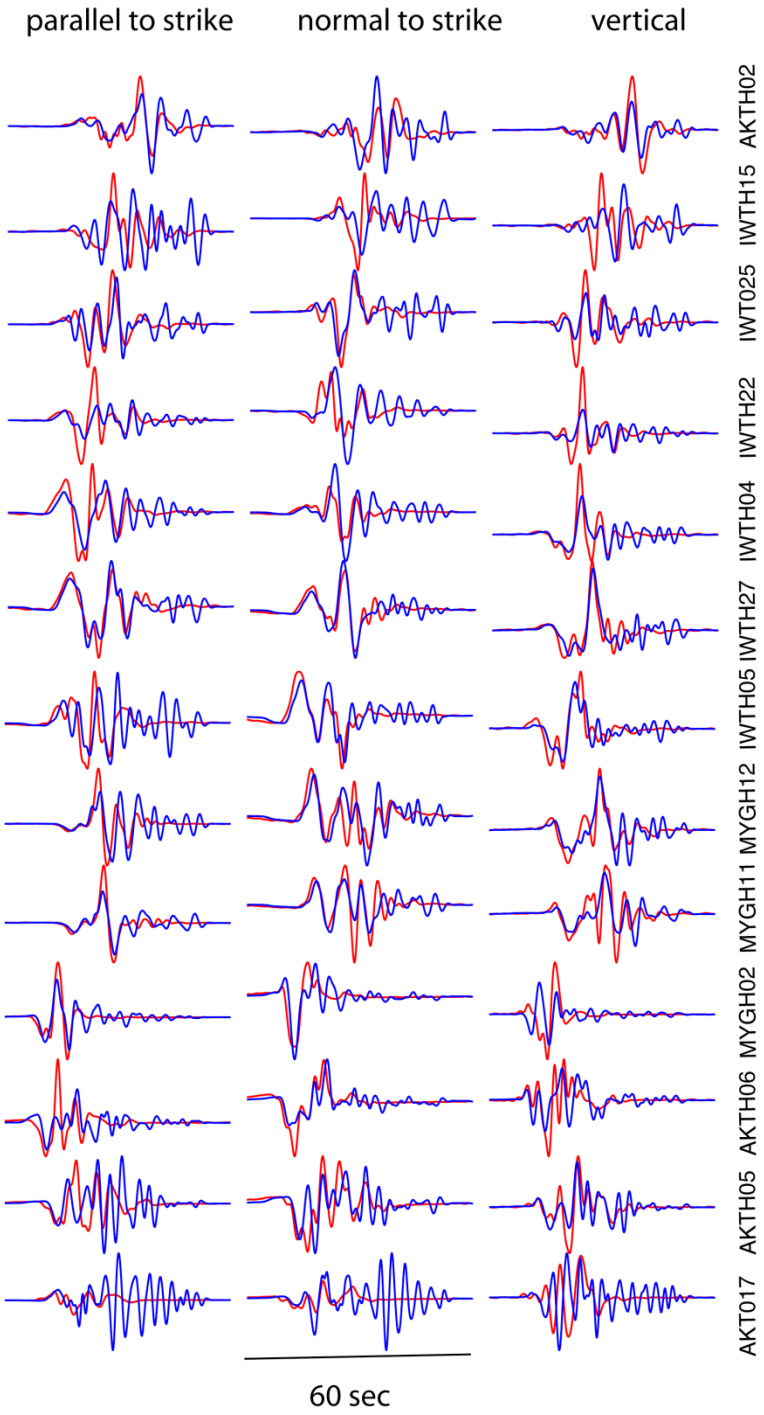

Figure S2. Comparison between observed velocity records (blue lines) and predicted waveforms (red lines) computed for the rupture model inferred from the inversion (Figure S1) at those stations used for the inversion procedure (figure 1). Data have been filtered in the 0.0-0.5 Hz frequency band.